



1 **Solar forced diurnal regulation of cave drip rates via phreatophyte evapotranspiration**

2

3 Katie Coleborn¹, Gabriel C. Rau¹, Mark O. Cuthbert², Andy Baker¹, Owen Navarre³

4 ¹*Connected Waters Initiative Research Centre, UNSW Australia, Kensington, NSW 2052*

5 *Australia*

6 ²*School of Geography, Earth and Environmental Sciences, University of Birmingham,*

7 *Edgbaston, Birmingham, B15 2TT, UK*

8 ³*School of Biology Earth and Environmental Sciences, UNSW Australia, Kensington, NSW*

9 *2052 Australia*

10

11 Corresponding author: Katie Coleborn

12 Email: k.coleborn@unsw.edu.au

13 Tel: +61434105636



14 **Abstract**

15 We present results of a detailed study of drip rate variations at 12 drip discharge sites in
16 Glory Hole Cave, New South Wales, Australia. Our novel time series analysis, using the
17 synchrosqueeze transform, reveals pronounced oscillations at daily and sub-daily
18 frequencies occurring in 8 out of the 12 monitored sites. These oscillations were not
19 spatially or temporally homogenous, with different drip sites exhibiting such behaviour at
20 different times of year in different parts of the cave. We test several hypotheses for the
21 cause of the oscillations including variations in pressure gradients between karst and cave
22 due to cave breathing effects or atmospheric and earth tides, variations in hydraulic
23 conductivity due to changes in viscosity of water with daily temperature oscillations, and
24 solar driven daily cycles of vegetative (phreatophytic) transpiration. We conclude that the
25 only hypothesis consistent with the data and hydrologic theory is that daily oscillations are
26 caused by solar driven pumping by phreatophytic trees which are abundant at the site. The
27 daily oscillations are not continuous and occur sporadically in short bursts (2-14 days)
28 throughout the year due to non-linear modification of the solar signal via complex karst
29 architecture. This is the first observation of tree water use in cave drip water and has
30 important implications for karst hydrology in regards to developing a new protocol to
31 determine the relative importance of trends in drip rate at different timescales and to infer
32 karst architecture. Our findings support a growing body of research exploring the impact of
33 trees on speleothem paleoclimate proxies.


34 **1. Introduction**

35 Karst architecture determines the flow and storage of water from the surface to the
36 underlying cave and is a major influence on drip discharge. Karst systems are characterised
37 by three principle flow types. Primary flow occurs where the water travels through the
38 primary porosity of the rock matrix, secondary flow pathways are characterised by water
39 transported along fractures in the bedrock and tertiary flow pathways consist of conduits
40 enlarged by dissolution. The dominance of a particular flow regime can be influenced by the
41 age of the limestone, for example, older limestone tends to be more heavily karstified (more
42 fractures and enlarged conduits) with a lower primary porosity due to marmorisation. The
43 relationship between karst architecture and delivery of water to cave drip discharge sites
44 has been studied to constrain uncertainty in paleoclimate studies (Bradley et al., 2010;
45 Markowska et al., 2015), identify suitable speleothems as climate archives (McDonald and
46 Drysdale, 2007) and in conjunction with drip water geochemistry to determine water
47 residence times in karst aquifers (Fairchild et al., 2000; Tooth and Fairchild, 2003; Treble et
48 al., 2013b). Recent research into drip hydrology and fluctuations in drip rate have used
49 hydrological response to characterise flow paths. For example, Markowska et al., (2015)
50 used statistical analysis of drip hydrology data to identify storage flow, in both the epikarst
51 and overlying soil, to develop conceptual models of a karst system.





52 Over a timescale of months to years, fluctuations in drip discharge are typically driven by
53 seasonal variation in water availability (Hu et al., 2008; Sondag et al., 2003) and long-term
54 climate forcings such as the North Atlantic Oscillation or El Niño-Southern Oscillation
55 (McDonald, 2004; Proctor et al., 2000). On a daily to weekly timescale, drip rate responds to
56 individual rainfall events (Baldini et al., 2012) and barometric changes (Genty and Deflandre,
57 1998; Jex et al., 2012; Tremaine and Froelich, 2013). Tremaine and Froelich (2013) found
58 weekly and daily fluctuations at one drip site where an increase in barometric pressure
59 decreased volumetric drip rate. This was attributed to atmospheric tides, the heating and
60 cooling of the atmosphere, as the diurnal cycles occurred at two hours before the solar
61 noon (S1) and solar midnight (S2) each day. The cave was situated in poorly to moderately
62 indurated Oligocene limestone with a high likelihood of primary porosity (Scott, 2001). Jex
63 et al. (2012) observed a negative correlation between weekly barometric pressure changes
64 and drip rate at two out of forty drip sites monitored at the base of a paleokarst feature in
65 the marmorised and fractured Devonian limestone at Cathedral Cave, NSW. One drip
66 discharge site had a relatively strong anti-correlation ($R=-0.52$) after accounting for a 40 hr
67 time lag. This relationship was attributed to a two-phase flow, where pressure fluctuations
68 expanded and compressed air bubbles in the water held within the paleokarst in the
69 unsaturated zone.

70 Non-linear and chaotic behaviour of drip discharge has been observed over very short
71 (second to minutes) timescales. Chaotic drip regimes were first noted by Genty and
72 Deflandre (1998) in the Devonian limestone of southern Belgium (Genty and Deflandre,
73 1998). Chaotic and non-linear drip responses were also observed at an event-scale in the
74 fractured-rock limestone of Cathedral Cave, NSW (Mariethoz et al., 2012). These were
75 attributed to the filling and draining of subsurface karst stores within a recharge event, with
76 increasing homogenisation of flow with the filling of the stores. Baker and Brunndon (2003)
77 observed non-linear responses to rainfall in multi-year drip time series from a fractured rock
78 (Carboniferous limestone) in Yorkshire, UK. With the exception of Tremaine and Froelich
79 (2013), daily fluctuations have not been observed in cave drip water hydrology. 

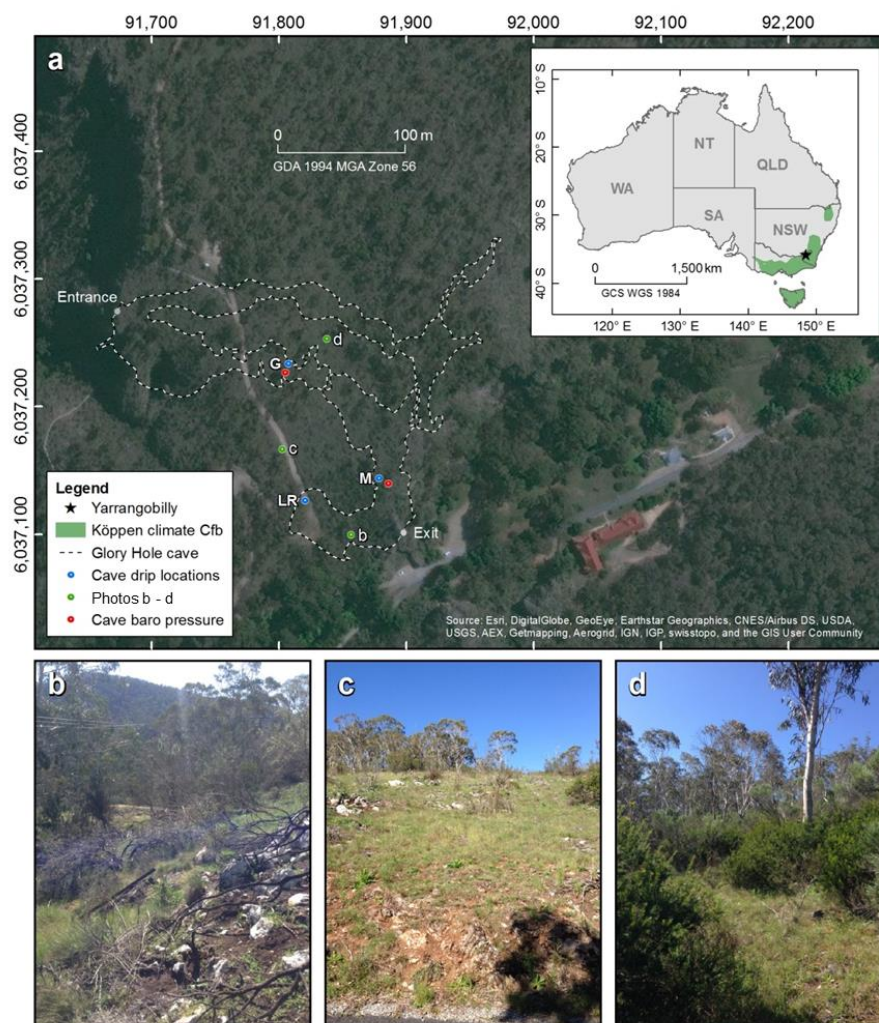
80 In this paper we aim to increase our understanding of karst architecture by using a novel
81 approach, the synchosqueeze transform, to analyse drip discharge time series from 12 drip
82 discharge sites in Glory Hole Cave, SE Australia. This analysis allows us to characterise daily
83 and sub-daily fluctuations in drip rate and identify the processes driving these oscillations.



84 **2. Field site and methods**

85 **2.1 Glory Hole Cave at Yarrangobilly Caves National Park**

86 Glory Hole Cave is part of the Yarrangobilly Caves National Park located in the Snowy
87 Mountains, New South Wales, Australia (35°43'29.3"S 148°29'14.9"E) at an elevation of 980
88 m **AHD**. The Snowy Mountains forms part of the Great Dividing Range, a mountainous
89 region stretching along the eastern seaboard from Queensland to Victoria. The region is
90 sub-alpine and the climate is classified as temperate montane with mild summers and no
91 dry season (Köppen climate classification Cfb) (Peel et al., 2007; Stern et al., 2012).



92

93 Figure 1 location of Yarrangobilly Caves in New South Wales, Australia with photos of
94 surface vegetation b-d. Extent of Köppen climate zone is from Peel et al. (2007).



95 Glory Hole Cave is formed of two main sections connected by a narrow constriction ~2 m x 6
96 m. It is ~243 m in length and is ~100 m at its widest point. The cave extends more than 40 m
97 below the surface in an unsaturated zone of westward sloping limestone bedrock. The cave
98 is situated within a formation of massive limestone approximately 12 km long and on
99 average 1 km wide (Worboys, 1982). The limestone is typical of south-eastern Australian
100 limestone; it is Silurian, highly fractured and marmorised with little primary porosity. The
101 bedding planes of the limestone are generally obvious with a westward dip (Adamson and
102 Loudon, 1966). It is likely that Glory Hole Cave was formed by water running off less
103 permeable rocks to the east of the limestone, sinking to the water table and rising through
104 large springs close to the Yarrangobilly River (Spate, 2002) which is situated in a gorge in
105 <100 m west of the cave entrance.

106 The vegetation is classified as sub-alpine open snowgum (*Eucalyptus pauciflora subsp.*
107 *pauciflora*) and black sallee (*E. stelullata*) woodland.

108

109 **2.2 Cave and surface monitoring**

110 Drip discharge rate was recorded at 12 drip sites in three locations (Fig. 1 and Table 1)
111 within Glory Hole Cave using Stalagmate© drip loggers between December 2012 and
112 September 2015, and monitoring is ongoing. Drip loggers recorded the frequency of drips
113 falling onto the surface of the sealed box containing an acoustic sensor in 15 min intervals.
114 The number of drips were converted to ml min⁻¹, assuming that 1 drip equals 0.19 ml
115 (Collister and Matthey, 2008). Recently, automated drip loggers have been widely used in
116 cave hydrology research (Cuthbert et al., 2014b; Hu et al., 2008; Mahmud et al., 2015;
117 Rutledge et al., 2014; Treble et al., 2013a) as they provide a more convenient and efficient
118 way of recording higher temporal resolution data than traditional drip counting methods.

119




120

121 Table 1 Summary of drip sites and location within cave as indicated in Fig. 1, the mean and
 122 standard deviation (std) of total flow volume and maximum and minimum drip rate in
 123 summer (December- February) and winter (June- August).

Site	Location	Total flow volume (L)				Drip rate (ml min ⁻¹)			
		Summer		Winter		Summer		Winter	
		mean	std	mean	std	Maximum	Minimum	Maximum	Minimum
G1	G	72.67	9.21	209.58	107.78	19.51	1.84	56.75	0.00
G3		23.76	10.13	115.44	8.37	7.00	0.00	34.43	0.00
G6		3.73	1.90	16.45	0.10	1.43	0.10	4.10	0.65
G8		6.36	0.49	5.81	0.16	1.11	0.00	0.96	0.34
G10		32.47	23.08	104.54	73.58	9.97	0.04	27.27	0.00
G12		6.57	5.71	9.74	4.39	1.68	0.00	2.04	0.43
LR1	LR	32.31	23.93	98.62	7.39	58.30	0.00	57.77	0.00
M1	M	0.29	0.18	0.47	0.00	0.13	0.00	0.11	0.00
M2		7.67	12.85	120.09	21.21	42.53	0.00	74.30	0.00
M4		0.88	1.47	33.95	5.17	4.02	0.00	28.45	0.00
M10		24.53	34.68	127.79	51.36	13.95	0.00	27.56	0.00
M13		7.33	5.05	67.03	6.60	12.40	0.09	41.80	0.92

124

125 Barometric pressure and air temperature were recorded at two locations within the cave
 126 (Fig. 1) using Solinst level loggers at 15 min intervals from January-September 2015.
 127 Precipitation (accuracy ± 4% of total), wind speed (accuracy ± 0.1 kph), relative humidity
 128 (accuracy ±2%), air temperature (accuracy ± 0.5 °C) and barometric pressure (accuracy: ±1.0
 129 hPa/ mb) were measured with a Davis Vantage Pro 2 weather station <1 km from Glory Hole
 130 Cave at 15 min intervals and data stored using a Datataker DT80 data logger. Solar radiation
 131 was derived from satellite imagery processed by the Bureau of Meteorology from the
 132 Geostationary Meteorological Satellite and MTSAT series.

133 Daily evapotranspiration was estimated using ETo Calculat  software developed by the
 134 Land and Water Division of the Food and Agriculture Organisation of the United Nations
 135 <http://www.fao.org/nr/water/eto.html>. The software is based on the Penman-Monteith
 136 equation and is a physically-based method with physiological and aerodynamic parameters.
 137 The climate parameters used were air temperature (mean, maximum and minimum),
 138 relative humidity (mean, maximum and minimum), wind speed and solar radiation. Daily
 139 evapotranspiration data was only available for the period 19/12/2012-03/07/2014 due to a
 140 malfunction in the weather station post-July 2014. Lag time analysis involved the manual
 141 calculation of the difference between the timing of minimum daily drip rate and the timing
 142 of maximum evapotranspiration during periods of daily drip rate oscillations. In the absence
 143 of sub-daily evapotranspiration data, the timing of maximum evapotranspiration was
 144 assumed to be 1 pm (Burgess, 2001).



145



146 **2.3 Spectral analysis of cave drip discharge rates**

147 Synchrosqueezing was used to analyse the frequency-time content of the cave drip
148 discharge rate. Daubechies et al (2011) first presented the synchrosqueeze transform (SST)
149 as an empirical mode decomposition like tool for disentangling a complex signal into
150 approximately harmonic components. SST combines the advantages of the wavelet
151 transform in regards to frequency resolution with the frequency reallocation method (Auger
152 and Flandrin, 1995) in order to reduce smearing when mapping out the frequency-time
153 content of a complex signal. Thakur et al (2013) adapted the transform to discretised data
154 and developed a MATLAB Synchrosqueeze Toolbox (available for download:
155 <https://web.math.princeton.edu/~ebrevdo/synsq/>) which efficiently implements the
156 algorithm and offers a log2 frequency resolution. They further tested the robustness
157 properties of SST and found that it precisely estimated key signal components, and that it
158 was stable against errors and noise (Thakur et al., 2013).

159 Using SST, spectral plots were created from drip discharge rate time series as well as their
160 surface weather related drivers (barometric pressure and air temperature). These plots
161 allowed visual identification of key frequency components as well as chaos, i.e. lack of
162 regular oscillations identified as signals with varying amplitude and frequency over time.
163 Drip discharge rate oscillations could be defined as continuous periods of a) stable 1 cycle
164 per day (cpd) frequency, b) stable 1 cpd and 2 cpd frequency, c) chaos. These spectral
165 “fingerprints” were used to identify and mark periods of continuous occurrence in the drip
166 discharge dataset.

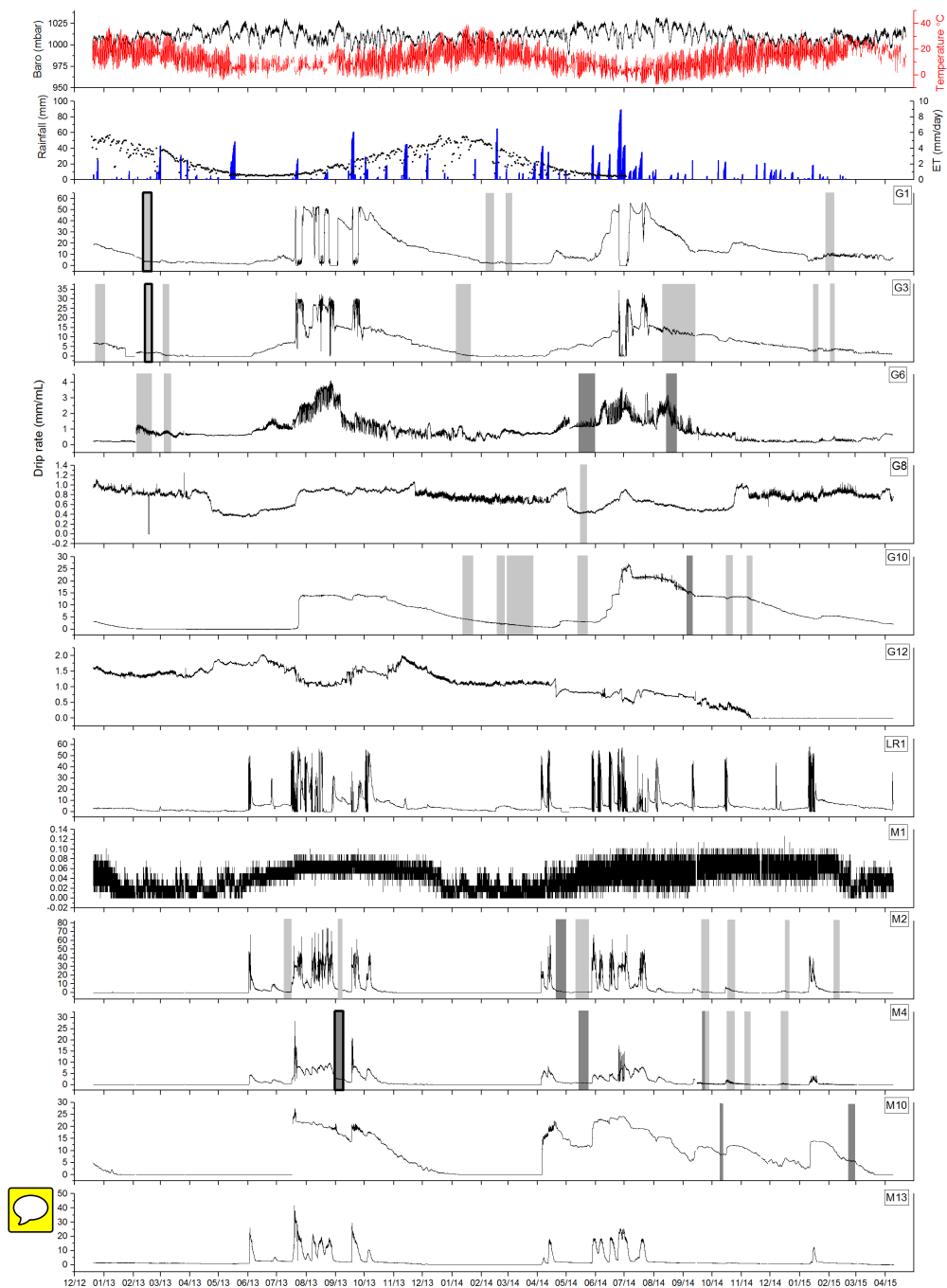


167

168 **Results**

169 **3.1 Drip discharge rate time series**

170 The drip discharge time series are presented in Fig. 2. The drip discharge sites are spatially
171 clustered in three groups within the cave (Fig. 1 and Table 1). Sites with the G prefix are
172 located near the main entrance of the cave on the western side. The location is highly
173 decorated with speleothems. M sites are located in the middle section of the cave in a large
174 chamber with a high ceiling populated by soda straw formations. Location LR1 is situated
175 near the cave exit at the top of a flow stone.



176

177



178 Figure 2 Drip discharge rate time series for all drip sites in Glory Hole Cave with periods
179 where daily fluctuations occur highlighted in light grey (1 cpd) and dark grey (1 cpd and 2
180 cpd). The time periods examined in more detail in Fig. 3, 4 and 5 are indicated by bolder
181 outline. Daily evapotranspiration (19/12/2012- 03/07/2014), rainfall, barometric, air
182 temperature and are also shown.

183 The drip discharge rate at G1 and G3 varies seasonally, with higher drip rates in winter, total
184 flow volume of 133.37 L and 109.52 L, respectively, than summer (64.56 L and 14.1 L,
185 respectively). Drip rate increases in response to rainfall events during the wet season and
186 gradually decreases through the drier part of the year. Drip rate is lowest during April and
187 May and highest during June and July. Similarly, G6 exhibits seasonal variation with a higher
188 volume of discharge during the winter than summer. The drip rate at G10 increases sharply
189 from 0.14 ml min⁻¹ on 21/07/2013 to 13.75 ml min⁻¹ on 29/07/2013, this drip rate is
190 consistently sustained for 3 months indicated by the flat topped hydrograph (Fig. 2). From
191 July 2013 onwards, the drip rate gradually decreases until June 2014 where it increases
192 sharply again by an order of magnitude from 2.03 ml min⁻¹ on 3/06/2014 to 24.96 ml min⁻¹
193 on 4/07/2014. In May 2014, the drip rate again rapidly increases at G10 from 0.142 ml min⁻¹
194 to 21.59 ml min⁻¹ on 18/04/2014 and then proceeds to gradually decline until April 2015
195 where it reaches baseline conditions. M10 exhibits similar behaviour with a low baseline
196 drip rate which increases sharply during July 2013 and is sustained for ~3 months, however,
197 the elevated drip rate decreases more rapidly than G10, returning to baseline conditions in
198 January 2014. M1 has a very low drip rate ranging from 0- 0.13 ml min⁻¹ and is seasonally
199 variable with higher drip rates during the winter. LR1, M2, M4 and M13 are very responsive
200 to infiltration events and are characterised by a 'flashy' flow type, evidenced by the
201 frequent spikes in drip rate. G12 has a low discharge rate which gradually decreases over
202 the monitoring period until the site dries up completely in November 2014. There are small
203 variations in drip rate that are not associated with rainfall events or seasonal drying. G8 is
204 the only site which has a lower total flow volume during the winter (2013= 5.92 L; 2014= 5.7
205 L) than summer (2014= 6.39 L; 2015= 6.84 L).

206

207 3.2 Characterisation of oscillations in the drip discharge rate

208 Daily fluctuations in drip discharge rate were identified in eight out of twelve sites using SST.
209 There was no connection between the sites that did not exhibit the fluctuations with
210 respect to spatial location, flow volume or flow regime type. The temporal and spatial
211 pattern of daily oscillations are shown by the grey shaded areas in Fig. 2. The length of time
212 the signal is present varied temporally for each drip site. For example, there was a strong 1
213 cpd signal in the drip water at G1 for 10 days in February 2013 whereas in January 2014 1
214 cpd fluctuations only lasted 5 days. The timing of when the signal occurs on an annual scale
215 varied within and between drip sites. For example, a 1 cpd signal only occurred during the
216 first 3 months of the year for G1, whereas a 1 cpd signal occurred sporadically at G3

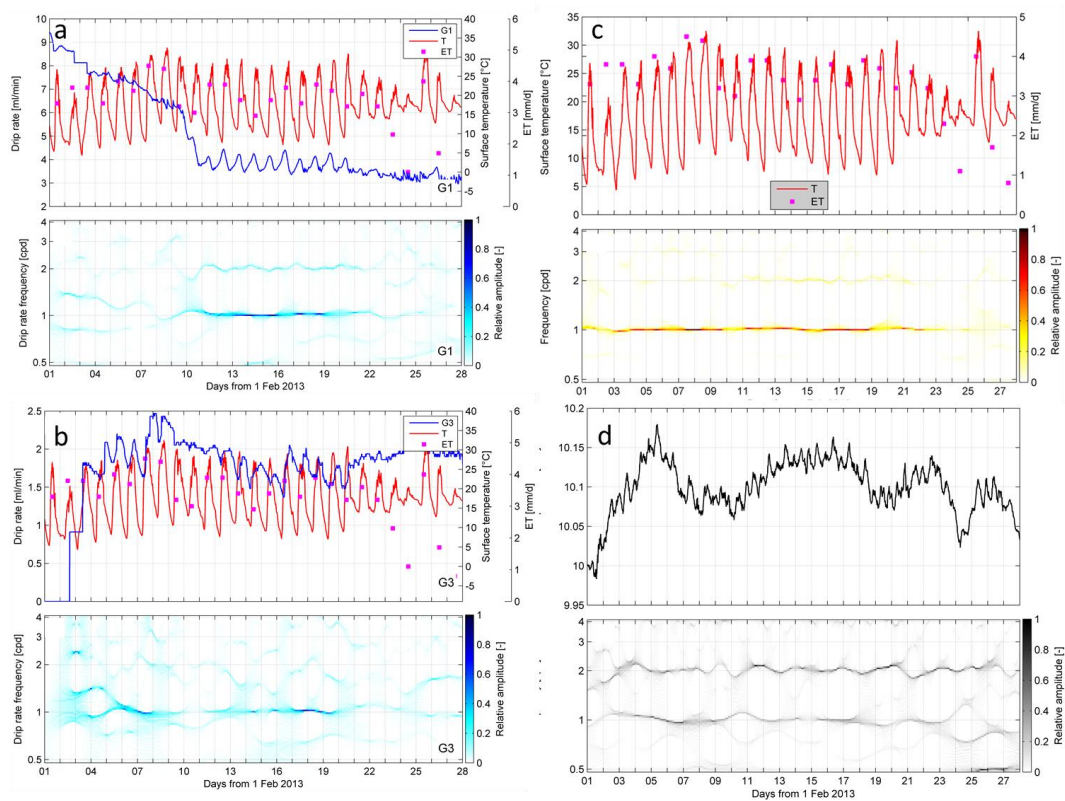


217 throughout the calendar year (December 2012, February and March 2013, January 2014,
218 September 2014, January 2015).

219 The daily timing of minimum and maximum drip rates varied within and between individual
220 drip sites. At G3 the 1 cpd minimum and maximum drip rate generally appeared between
221 12- 9 am and 3pm-12am, respectively. The minimum drip rate lagged 11-20 hours behind
222 the timing of maximum evapotranspiration, which Burgess et al (2001) estimated to be 1
223 pm. Daily oscillations were only observed once at G8 between 14-21/05/2014 with
224 minimum drip rate appearing 3-9 am and maximum drip rate appearing between 12-9 pm.
225 G6 exhibited a similar pattern with the exception of May and August 2014 where an
226 additional 2 cpd signal was observed with the second peak following 3-6 hours later. Similar
227 patterns of minimum drip rate lagging 11-20 hours behind the maximum daily
228 evapotranspiration were exhibited at G10 (with weak 2 cpd between 5-16/10/2013) and M2
229 (with weak 2 cpd between 20-28/04/2014). Both 1 cpd and 2 cpd signals were observed at
230 M10 for all the periods of drip rate oscillation with the larger peak occurring in the
231 afternoon between 3-6 pm and the smaller peak between 12-3 am, minimum drip rate
232 appeared consistently between 6-9 am. In contrast, minimum drip rate at G1 was observed
233 between 12-9 pm and maximum drip rate between 6-9 am indicating a lag time of ≤ 9 hours
234 behind peak evapotranspiration. M4 was unique in that minimum drip rate are recorded
235 between 6-9 am until October 2014 when it switches to 12-9 pm.

236 1 cpd and 2 cpd signals can occur concurrently, for example, at M4 between 1-9/9/2013
237 (Fig. 4). This trend, where the 2 cpd is weaker than the 1 cpd is consistent across all sites
238 where the two signals coincide. The 2 cpd signal can be visually determined in the raw drip
239 rate data by a second smaller peak (Fig.4). Examples of characteristic SST plots alongside the
240 corresponding raw drip rate and surface temperature data will be discussed in greater detail
241 below. All SST analyses have been plotted in the SI.

242



243

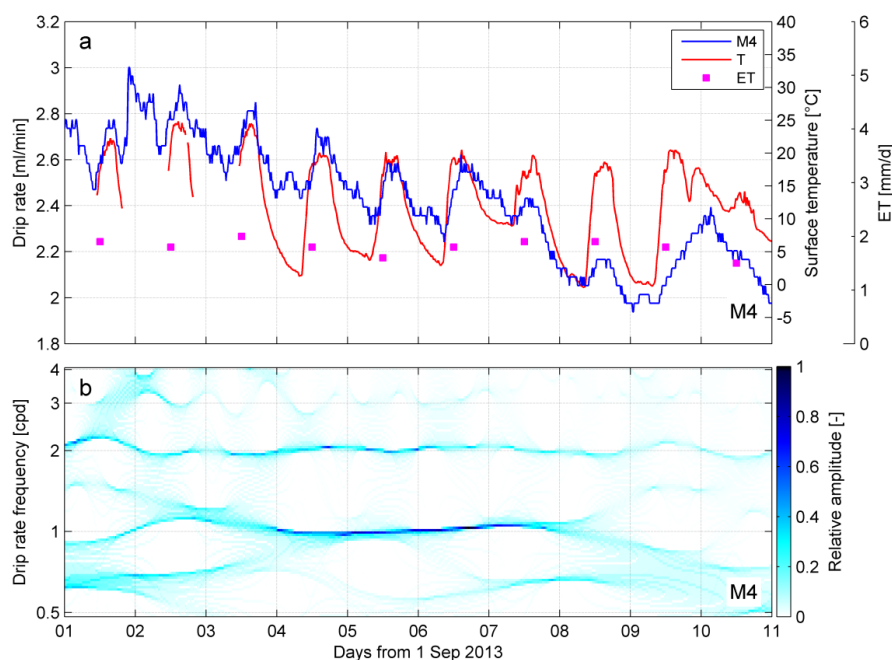
244

245 Figure 3 shows the raw drip rate, evapotranspiration and surface temperature data with the
246 corresponding drip rate synchrosqueezing plot for time periods where a 1 cpd signal is
247 present for sites a) G1 and b) G3 c) surface air temperature and evapotranspiration and d)
248 barometric pressure for period February 2013.

249



250



251

252 Figure 4 shows the raw drip discharge data, evapotranspiration, surface temperature and
253 synchrosqueeze transform (SST) plot of the drip discharge for site M4 from 1-
254 11/09/2013. SST identified a 1 cpd oscillation in drip rate between 08/02/2013 and
255 21/02/2013 at G1 and G3 (Fig. 3a, b). At G1 (Fig. 3a), the signal was initially chaotic, but
256 from 08/02/13- 21/02/13 the drip rate oscillates sharply at 1 cpd. The maximum drip rate
257 ranging from 4.03-3.75 ml min⁻¹ occurred between 9:18 and 10:27 and the minimum drip
258 rate ranging from 3.34 -3.75 ml min⁻¹ occurred between 18:39 and 21:27. The signal was
259 chaotic from 21/02/2013.

260 The drip rate at G3 (Fig. 3b) oscillated at 1cpd for 8 days from 12/02/13-20/02/13. In
261 contrast to G1, the maximum drip rate appeared in the evening and the minimum drip rate
262 occurred in the morning. The maximum drip rate ranging from 1.63 -2.01 ml min⁻¹ occurred
263 between 20:21 and 00:40 and the minimum drip rate ranging from 0.36-0.48 ml min⁻¹
264 occurred between 9:03 and 11.36 with the exception of 15/02/13 and 18/02/13 where it
265 appeared at 14:06 and 12:57, respectively. Similarly to G1, the 1 cpd trend descended into
266 chaos from 20/02/13 onwards. The maximum drip rate occurs between 14:23 and 22:45 and
267 ranged from 0.53 to 1.14 ml min⁻¹. The minimum drip rate occurred between 01:18 and
268 11:32 and ranged from 0.228 to 0.95 ml min⁻¹.

269



270 From 01-27/02/13, daily barometric pressure peaked between 8:30-9:00 with a magnitude
271 of ~1-5 mbar with a smaller second peak between 20:00-22:00 with a magnitude of 1-3
272 mbar (Fig. 3c). There were larger changes in air pressure on a mesoscale with peaks in air
273 pressure on 16/02/13, 22/02/13, 26/02/13 and minimum air pressure on 19/02/13,
274 24/02/13 and 28/02/13. The air pressure changes in these cycles were as much as 15-20
275 mbar. The drip rate at G1 and G3 did not appear to be affected by the daily or weekly
276 changes in air pressure. For example, when air pressure decreased dramatically on 27/02/13
277 (Fig. 3c) there was no substantial change in drip rate at either G1 or G3.

278 Insolation drives daily cycles in surface air temperature with maximum temperatures
279 recorded between 11:30-16:00 and minimum temperatures recorded between 4:00-8:00
280 (Fig. 3d). The difference in daily minimum and maximum air temperature varied greatly. For
281 example, between 12- 20/02/2013 the difference was 17.05-22.2 °C whereas between 21-
282 27/02/2013, the temperature difference was as little as 4.5 °C. Evapotranspiration ranged
283 from 0.8- 4.5 mm/day and was relatively high from 1-23/02/2013 with a slight downward
284 trend which then decreased sharply on 23/02/2013 and 24/02/2013 to 2.3 mm/day and 1.1
285 mm/day, respectively. Evapotranspiration had a strong correlation with maximum daily air
286 temperature ($R^2= 0.59$, p-value <0.05).



287 4. Discussion

288 4.1 Cave drip rate and karst architecture

289 The complexity of the Glory Hole Cave karst system is evident in the variety of drip regimes.
290 For example, the drip rate at G1, G6 and G3 is seasonally driven with high discharge rates
291 during the wettest period of the year. In contrast, drip discharge at G10 and M10 is likely
292 driven by a storage component which discharges via a permeable pathway which limits the
293 store at a particular level during wet periods. The drip site is fed via the main water store
294 rather than the overflow pathway itself (Baker et al., 2012; Bradley et al., 2010). Sites LR1,
295 M4, M13 and M2 behave similarly in that they are all very responsive to rainfall events and
296 have low base flows during periods of low rainfall. The response to rainfall events occur
297 within 24 hours across these sites. Calculated flow volumes indicate the storage capacity of
298 the stores feeding the discharge sites. For example, there was an infiltration event on
299 01/06/2013 which caused a dramatic increase in drip rate for sites LR1, M2, M4 and M13.
300 The flow volumes for each site from the start of the event to the point where the discharge
301 returns to a constant rate are as follows LR1 (1.60 L), M4 (2.99 L), M13 (8.09 L) and M2
302 (11.30 L). The length of the recession limb is indicative of the speed at which the store
303 drains. For example, the decay in drip rate is 12 days for site M2 compared to 4 days for
304 M13. The time it takes for the store to drain is not dependent on flow volume, as M13 has a
305 flow volume of more than 5 times that of site LR1 but they both have drainage periods of 5
306 days. The discrepancy in drainage time could indicate variation in flow pathway length
307 between sites. G8 is the only site with a relatively lower total flow volume during winter
308 than summer. M1 has a low drip rate that shows a small seasonal fluctuation but does not
309 visibly respond to individual events. This site is likely being fed by a store that is large
310 enough to assimilate short term inputs from the surface without impacting drip rate. This
311 type of store has been described in a karst hydrological model by Markowska et al. (2015).



313 4.2 Daily oscillations in drip rate

314 Constant frequency oscillations in drip discharge (1 cpd and 2 cpd) occur sporadically
315 throughout the monitoring period December 2012- April 2015 at 8 out of 12 monitored drip
316 sites. This phenomenon could be explained by a number of daily drivers including variations
317 in pressure gradients between karst and cave due to cave ventilation effects, atmospheric
318 and earth tides, or variations in hydraulic conductivity (due to changes in viscosity of water
319 with daily temperature oscillations), and solar driven daily cycles of vegetative
320 (phreatophytic) transpiration. These drivers are now considered in turn.



321 4.2.1. Cave ventilation effects

322 A student's t-test showed that there was no significant difference between surface air
323 pressure and cave air pressure for the monitoring period 19/01/2015-08/09/2015 (p-value=



324 $3.95 \cdot 10^{-6}$, $n=8939$). This indicates that cave air exchange (“breathing” or ventilation) is very
325 efficient and consequently that variations in air pressure between the cave and surface can
326 be ruled out as driving the fluctuations in drip rate.

327

328 **4.2.2. Barometric loading**

329 Atmospheric tides are caused by changes in air pressure due to the heating and cooling of
330 air masses during the day and night. Correlations between atmospheric tides and drip rates
331 can occur since increases (decreases) in atmospheric pressure at the ground surface are
332 partitioned into stress increase (decrease) in the soil/rock mass and pore pressure increase
333 (decrease) within the formation (Acworth et al., 2015). Drip rates could be affected if this
334 changes the pressure gradient between the groundwater in karst stores and the cave
335 (Tremaine and Froelich, 2013). Such a pressure imbalance is dependent on the
336 hydromechanical properties and karst architecture as well as the degree of pneumatic
337 connection between both the surface and the water table, and the surface and the cave at
338 the location of the drip. Maximum and minimum atmospheric pressure occur at the same
339 time each day (Fig. 3c).

340 Atmospheric tides were eliminated as a process to explain the daily oscillation phenomenon
341 for several reasons. Firstly, there was no relationship between drip discharge rate and the
342 longer term barometric changes caused by synoptic weather patterns (Fig. 4c). The
343 mesoscale fluctuations in pressure caused by synoptic weather patterns are an order of
344 magnitude higher than those caused by daily atmospheric tides. Since the drip rate did not
345 respond to pressure changes of this size, they will not respond significantly to changes of a
346 smaller magnitude at a higher frequency because higher frequency signals will be more
347 highly damped and lagged. Secondly, the timing of the daily maximum and minimum drip
348 rates in Glory Hole Cave varied within each drip site over time. For example, the peak
349 discharge time for site G6 varied between 13:24 and 19:48 for the period 11/08/2013-
350 25/08/2015. This finding contrasts with previous studies where drip rate is negatively
351 correlated with barometric pressure and responds to daily pressure changes linearly
352 (Tremaine and Froelich, 2013). However, this could indicate that the daily drip water
353 variations in Glory Hole Cave are being driven by a non-linear process and this is discussed
354 further below. Thirdly, the karst architecture of Glory Hole Cave is well-developed, has little
355 to no primary porosity and is unconfined. Hence, it is unlikely to exhibit barometric
356 responses such as seen in confined systems (Merritt, 2004), whereby pore pressure changes
357 due to barometric loading are substantially lower than the change of cave air pressure.

358

359 **4.2.3. Earth tides**



360 Earth tides are solid deformations of the Earth's surface caused by the gravitational pull of
361 the moon and sun (Merritt, 2004). It has been previously shown that earth tides can cause
362 regular oscillations in groundwater level if the aquifer is sufficiently confined (Acworth et al.,
363 2015). However, at Glory Hole Cave this process can be ruled out due to the unconfined
364 conditions, the fact that the compressibility of limestone is smaller than that of water, and
365 because fluctuations in pressure caused by earth tides are so small.

366

367 4.2.4. Temperature driven viscosity influences on hydraulic conductivity

368 The study site has large surface temperature variations, particularly in summer where day
369 time and night time temperatures can vary up to 31.1 °C. Consequently, the dynamic
370 viscosity of water could range from 0.8- 1.79 x 10⁻³ Pa s (based on a temperature range from
371 30-0 °C, respectively). However, the conductive propagation in diel temperature variations
372 are expected to be highly attenuated with depth (Rau et al., 2015) resulting in almost
373 complete damping by 1 m bgl. Furthermore, the daily temperature range within the cave
374 itself is just 0.08-1.53 °C, primarily due to air exchange moderated by conductive
375 equilibrium with the cave walls. The variation of water viscosity (which is inversely
376 proportional to hydraulic conductivity) is approximately 2 to 3 % per degree in the range
377 10 to 30 °C. Considering that the amplitude of a 1 cpd drip rate fluctuation can be as much
378 as 75 % of the maximum drip rate, the greatest anticipated change in hydraulic conductivity,
379 and therefore the drip rate (proportional to the hydraulic conductivity by Darcy's law), on a
380 daily cycle, is likely to be 2-3 orders of magnitude lower than the observed variation in drip
381 rate on a daily basis. We therefore conclude that the daily fluctuations in drip rate are
382 unlikely to be caused by variations in hydraulic conductivity due to changes in viscosity of
383 water.

384

385 4.2.5. Solar driven daily cycles of vegetative (phreatophytic) evapotranspiration

386 The timing of the daily drip rate signal appears to be associated with the difference in
387 maximum and minimum surface temperature. In the examples examined in more depth in
388 Fig. 3a-b, when the difference between the maximum and minimum temperature was high
389 (17.05-22 °C) and the evapotranspiration was relatively high (mean 3.6 mm/day) the 1cpd
390 signal was strong. Conversely, when the temperature difference was small (4.5-12.7 °C) and
391 the evapotranspiration was relatively lower (mean 2.2 mm/day), the 1 cpd signal dissolved
392 into chaos.

393 During periods when there are 1 cpd oscillations in drip rate, there is a relationship between
394 drip rate and surface temperature on a weekly timescale. For example, in Fig. 5 there is a
395 negative relationship between the daily moving averages for surface air temperature and
396 drip rate at G1 from 01-19/02/2014. We have demonstrated above that it cannot be air



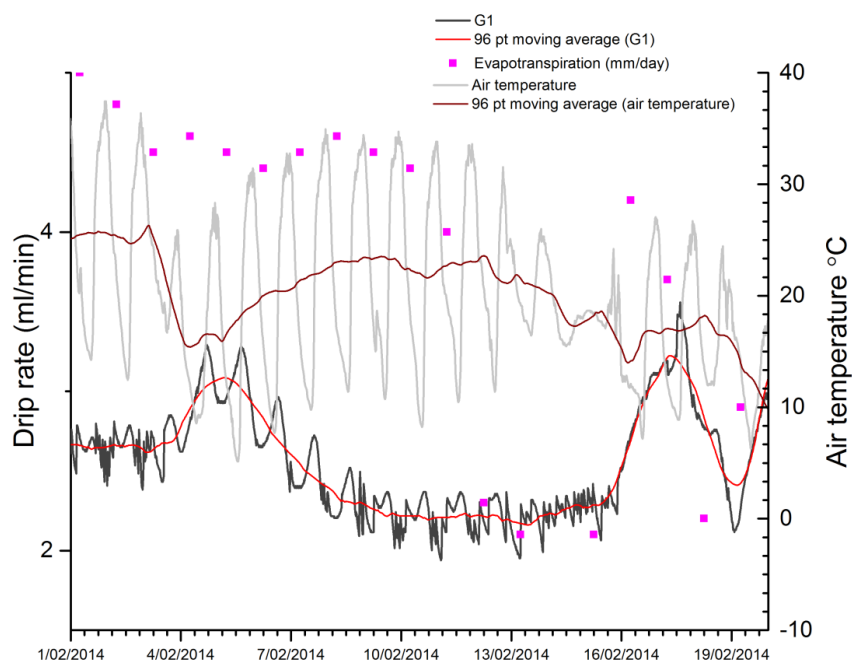
397 temperature driving the signal through either atmospheric tides or water viscosity changes.
398 However, the relationship between surface temperature variability and 1 cpd drip rate
399 oscillations could be explained if the association with diurnal temperature variability is due
400 to variations in solar radiation received at the surface, as it is solar radiation which primarily
401 drives photosynthesis and thus transpiration in vegetation. This is confirmed by the strong
402 positive relationship between daily solar radiation and evapotranspiration ($R^2= 0.59$, p-value
403 <0.05). Daytime solar radiation receipt is highest in the absence of cloud cover, because
404 there is no barrier to incoming long wave and short wave radiation which leads to the
405 heating of the earth's surface and atmosphere, resulting in higher air temperature. Due to
406 the lack of cloud cover, night-time cooling occurs because of the loss of heat through
407 outgoing long wave radiation, therefore periods of high daytime solar radiation are
408 characterised by large air temperature amplitudes. In comparison, solar radiation received
409 at the earth's surface is low in the presence of cloud cover. In this case, there is a smaller
410 temperature amplitude because clouds reduce the amount of incoming short wave and
411 longwave radiation during the day, reducing daytime temperatures and reduce the amount
412 of outgoing longwave radiation and effectively "insulating" the air at night leading to
413 relatively warmer temperatures at night.



414 During periods of high solar radiation, plants photosynthesise more and therefore use more
415 water. We hypothesise that firstly, tree water use was driving the intermittent daily
416 oscillations in drip discharge demonstrated by the relationship between daily to weekly
417 variations in surface air temperature and drip discharge and secondly, the sporadic nature
418 of the oscillations was driven by complexities in the karst architecture. It has been widely
419 accepted that tree water use causes fluctuations of the water table (Gribovski et al 2010;
420 Acworth et al 2015). However, this is the first study that shows tree water use affecting cave
421 drip water.



422 The area above the cave and in the small uphill catchment is dominated by *E. pauciflora* and
423 *E. stelullata* (Fig. 1). Eucalypt species have a bimodal root systems with shallow lateral roots
424 and vertically descending roots which penetrate into the profile to depths of up to 18 m,
425 with depth depending on soil characteristics and the degree to which the bedrock is
426 fractured/conduits developed (Crombie, 1992; Farrington et al., 1996). Hence, these trees
427 have the mechanism to abstract water from karst stores at depth which supports our theory
428 that tree water use causes daily oscillations in cave drip rate.

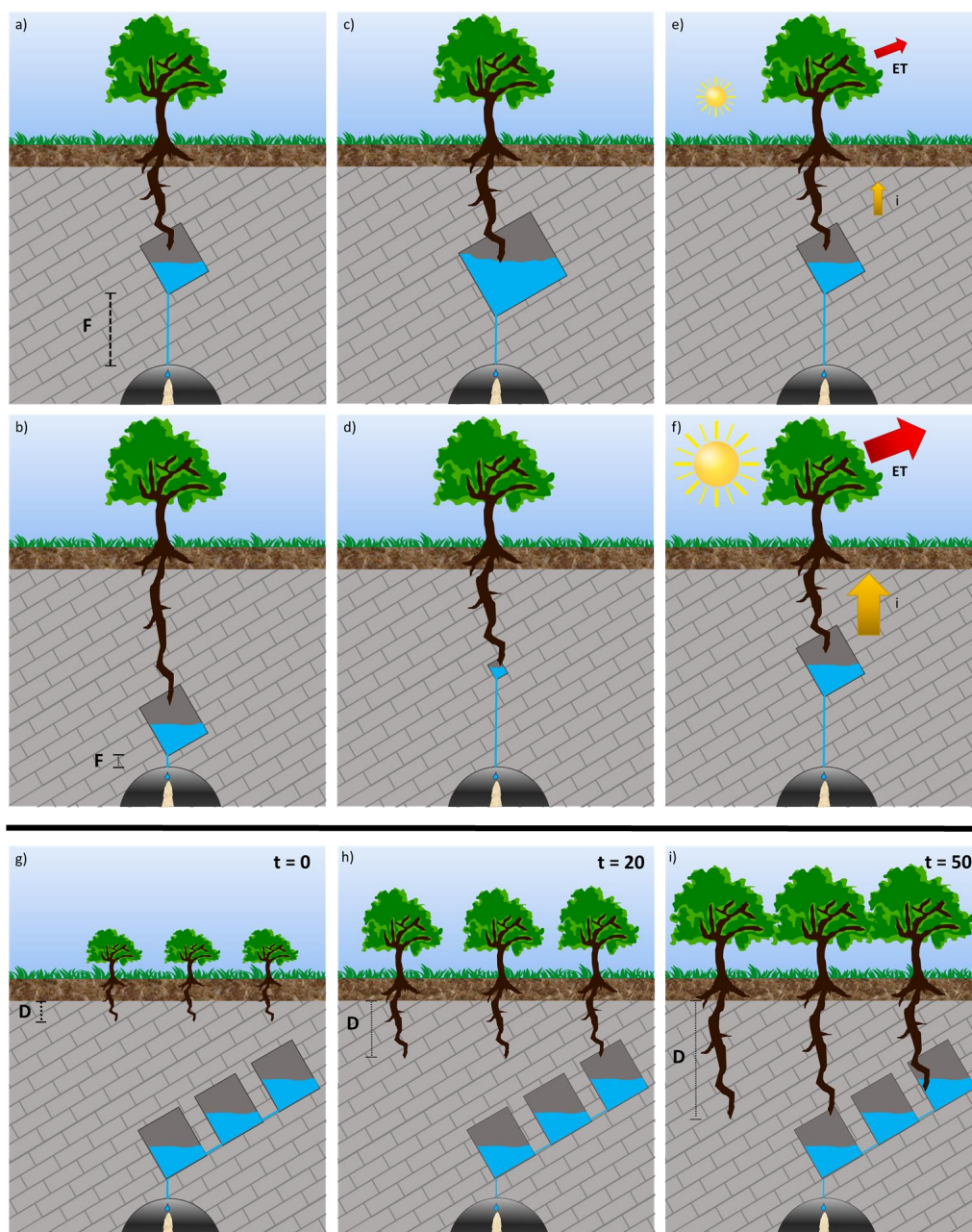


429

430 Figure 5 shows the surface air temperature, evapotranspiration and drip discharge rate with
431 the corresponding daily moving average for site G1 01/02/2014-19/02/2014.

432

433 Tree water use from deep roots increases with the need for the tree to obtain water, and
434 this will increase with increasing transpiration and solar radiation (O'Grady et al., 1999).
435 Maximum tree water use by the roots is therefore expected in the afternoon during the
436 period of maximum solar radiation, possibly lagged due to the time taken to hydraulically lift
437 the water. Conversely, minimum tree water use is expected at the end of night around 6am.
438 Burgess et al (2001) measured sap flow in Eucalypt tap roots, finding positive hydraulic lift
439 peaked around 1 pm and a negative hydraulic lift between 7pm- 7am. In consideration of
440 this, drip water that comes from fractures and stores which contain tree roots would be
441 expected to have a minimum drip discharge in the afternoon and maximum around sunrise.
442 In reality, we observe more complex daily drip oscillations, with peak drip rate occurring at
443 different times of the day and different times of the year. This is to be expected from a
444 karstified system with flow routed through a varied and complex fractured network.
445 Different scenarios driving daily oscillations in a karst system will be discussed in detail
446 below.



447
 448

449 Figure 6 shows a conceptual representation of tree water use from karst stores under
 450 different circumstances. a) and b) show different karst store-drip site flow path lengths (F)
 451 as the tree roots access karst stores at different depths; c) and d) show tree roots accessing
 452 karst stores with different volumes; the influence of annual insolation on evapotranspiration





453 (ET) and hydraulic lift (i) during winter and summer is shown in e) and f) respectively. Finally,
454 the increase in rooting depth (L) and access to deeper karst stores over time in years (t) is
455 explored in g-i.

456 The depth of a store could affect the timing of daily drip rate oscillations due to the delay in
457 tree water transport. For example, consider the hypothetical, identical trees with roots
458 intercepting identical karst stores or fractures at *different* depths in Fig. 6a and 6b. There is
459 likely to be a greater lag in drip response in Fig. 6a than Fig. 6b because of the longer flow
460 path-length (F) from the tree root to the cave drip site. Given that eucalypt tap roots can
461 penetrate to depths ranging from 5-20 m with tap root length depending on the depth of
462 accessible water (Carbon et al., 1980; Dawson and Pate, 1996) and the drip sites at Glory
463 Hole Cave are located 30-50 m below the surface, we can speculate that the minimum flow
464 path length between a taproot accessing the karst store and the drip site below could vary
465 from 10-45 m. In reality, it is difficult to calculate exact flow path length because of the
466 prevalence of lateral flow in heavily karstified systems. This has been demonstrated by
467 Markowska et al (2016) in a study where water spiked with a tracer was used to irrigate the
468 surface above a cave resulting in a response at discharge sites located 7 m laterally from the
469 irrigation location. At all drip discharge sites the minimum drip discharge rate is lagged by
470 12-18 hours from when we would expect the peak transpiration to occur at 1pm. The
471 exception is G1 where the minimum discharge rate occurs between 12-9 pm indicating a lag
472 time of ≤ 9 hours. We can hypothesise that G1 has a shorter path length from tree root
473 accessed store to cave discharge site than the other drip sites. This process could also
474 explain the unique case of M4 where the timing of minimum and maximum drip rate during
475 a 1 cpd oscillation switches in October 2014 (Fig. 2). We hypothesise that the change is due
476 to a shortening of the path length from root accessed store to cave discharge site as the tree
477 grows and increases its rooting depth, thus accessing a deeper water store.

478 The size of the karst store, or volume of water within the store, could determine whether
479 the daily oscillation is observable or not. Consider the conceptual Fig. 6c and 6d, where
480 identical trees have roots intercepting different karst stores at the *same* depth. We
481 hypothesise that a daily oscillation will only be observed when the tree water use is a
482 significant part of the total water store so a daily oscillation is more likely to be observed in
483 the smaller store (Fig. 6d) than a store with a larger volume (Fig. 6c). This is supported by
484 the fact that, generally, the daily oscillations are not exhibited during periods of high rainfall,
485 and consequently high drip discharge, as the tree use signal is more likely to be a smaller
486 fraction of the total water volume. Sites G1, G3 M2 and M4 have high seasonal discharge
487 rates during June-September as indicated by the multiple hydrograph peaks for the
488 corresponding sites in Fig. 2. There are no daily oscillations during these periods of peak
489 discharge at any of these sites. Daily oscillations coincide with the receding limb of the peak
490 at sites M4 (July and September 2013) and M4 (September 2013) as the drip rate decreases.
491 The influence of store volume on the presence of daily oscillations could also explain why
492 phenomenon is not observed at M1. In section 3.1 we discuss how the low, consistent drip



493 rate at M1 responds to seasonal drying but does not respond to individual rainfall events.
494 We propose that this site is fed by a store large enough to assimilate individual rainfall
495 events and the same line of reasoning could explain the lack of response to tree water use,
496 the volume of water extracted by tree roots is insignificant in relation to the large volume of
497 water in the store. The non-observance of daily oscillations during periods of high rainfall
498 could also be attributed to the redistribution of water by the roots from the saturated soil to
499 the unsaturated subsurface (Burgess et al., 2001)

500 Tree water use responds to annual variation in insolation. Consider Fig. 6e and Fig. 6f where
501 one tree root intercepts the same karst store over the course of a year. During winter (Fig
502 6e), there is less insolation than the summer (Fig 6f) therefore the rate of
503 evapotranspiration is lower. This means that in winter the hydraulic lift (i) is low or negative
504 and daily oscillations in drip discharge could be dampened or absent. Our analysis reveals
505 that only 2 out of 41 periods of 1 cpd oscillation occur during winter months June-August
506 (G6 between 14-24/8/13 and M2 between 8-13/7/2013).


507 In reality, there are multiple trees of different ages above the cave, further complicating the
508 flow variability. Figure 6g-i presents a conceptual representation of tree tap root length
509 increasing (L) as the tree grows and accesses deeper karst stores over 0-50 yr timescale (t).
510 This response to annual insolation and the interaction of multiple trees of varying ages could
511 explain why daily oscillations at an individual drip site occur one year and not the next, for
512 example at M10 there is a 1 cpd in December 2012 however, this oscillation does not occur
513 at the same time in 2013 or 2014. The mechanism in Fig. 6i could also explain why 2 cpd
514 signals are also observed, whereby multiple tree roots are accessing interconnected water
515 stores at different depths resulting in two separate cycles with differing lag times. The
516 occurrence of 2 cpd signals in drip rate could also be related to signal processing where if
517 the signal is not strictly sinusoidal there may be harmonics in the spectrum. This finding and
518 the interpretation is an area for further research.

519 **4.6 Implications for karst architecture and climate proxy modelling research**

520 Karst architecture controls flow regimes and drip discharge rates of water exfiltrating into
521 caves (e.g., Markowska et al., 2015). Flow rate influences speleothem climate proxies, such
522 as the $\delta^{18}\text{O}$ and concentration of solutes in drip water, through the dilution and mixing of
523 percolation waters prior to reaching the cave. It is important to distinguish between the
524 influence of karst architecture and climate-driven processes, such as drought, on discharge
525 so that paleoclimate proxy records from associated speleothems can be appropriately
526 constrained. This study has increased our understanding of karst architecture, information
527 which can be utilised in proxy-system models or forward models, approaches that are
528 increasingly used to understand cave drip rate variability and to model speleothem proxies
529 such as $\delta^{18}\text{O}$ (Bradley et al., 2010; Cuthbert et al., 2014a). Additionally, we propose that an
530 important part of any protocol for inferring karst architecture is 1) the incorporation of cave
531 drip rate monitoring with a minimum 15 min interval at multiple discharge sites for at least a



532 year and 2) the systematic investigation of daily, weekly and monthly timescales using
533 frequency analysis capable of showing frequency-time changes, such as the synchrosqueeze
534 transform (Daubechies et al., 2011) to infer karst flow processes and their relative
535 importance.

536 This is the first volumetric observation of tree water use in cave drip water. This supports a
537 growing number of studies examining the impact of trees on karst processes and
538 paleoclimate proxies. For example, tree root respiration provides a source of CO₂ for the
539 dissolution of limestone that is additional to that from soil and vadose zone microbial
540 respiration. Coleborn et al (2016) found that vegetation regeneration determined post-fire
541 soil CO₂ in a study investigating post-fire impacts on karst processes. Direct observations of
542 tree water use within the karst unsaturated zone implies the presence of root respiration, a
543 process which in turn affects drip water and speleothem ¹⁴C and δ¹³C composition (Fairchild
544 and Baker, 2012; Meyer et al., 2014; Noronha et al., 2015). Trees have been demonstrated
545 to have long-term effects on cave drip-water solute concentrations. Treble et al. (2015,
546 submitted) demonstrate long-term trends in drip water calcium and trace element
547 concentration, which they attribute to increasing solute concentration due to forest
548 regrowth and increased post-fire tree water use. Baldini et al (2005) infer an effect on
549 speleothem δ¹⁸O due to secondary forest regrowth after mining and Wong and Banner
550 (2010) found clearing surface vegetation changed drip water Mg/Ca and Sr/Ca. The findings
551 and suggested protocol in this study will inform the selection of speleothem specimens for
552 further research into the impact of tree water use on speleothem paleoclimate proxies. 

553 5. Conclusions

554

555 We demonstrated a novel method of analysing recurring patterns in cave water drip rate
556 using the synchrosqueezing transform (SST). Our analysis revealed daily and sub-daily
557 oscillations with variable temporal and spatial signatures. We tested competing hypotheses
558 for causes of daily oscillations using drip rate, barometric and temperature data. The only
559 hypothesis which all the data and hydrodrologic theory were consistent, was that daily
560 fluctuations in drip rate were driven by tree water use. We proposed that the complexity of
561 flow pathways in the karst system accounted for the spatial and temporal variation in the
562 daily fluctuations of drip rate. This was explored in detail using conceptual models. The
563 results have wider implications for karst research including providing a new protocol for
564 inferring karst architecture and informing selection of speleothem specimens for tree water
565 use paleoclimate studies.

566

567 Author contribution



568 KC, MOC, GCR and AB wrote the manuscript, discussed the results and implications and
569 commented on the manuscript at all stages. KC, AB and ON collected data. GCR performed
570 the SST analysis and generated the SST figures. GCR and ON created the location map. KC
571 generated other graphs and conceptual figures.

572 Acknowledgements

573 We acknowledge that Katie Coleborn was supported the Australian Research Council
574 (LP130100177). Mark Cuthbert was supported by Marie Curie Research Fellowship funding
575 from the European Community's Seventh Framework Programme [FP7/2007-2013] under
576 grant agreement n.299091. We would also like to thank Stuart Hankin for allowing us access
577 to the weather station data and the National Parks and Wildlife Service staff at Yarrangobilly
578 Caves. Solar exposure data derived from satellite imagery processed by the Bureau of
579 Meteorology from the Geostationary Meteorological Satellite and MTSAT series operated by
580 Japan Meteorological Agency and from GOES-9 operated by the National Oceanographic &
581 Atmospheric Administration (NOAA) for the Japan Meteorological Agency

582 References

- 583 Acworth, R. I., Rau, G. C., McCallum, A. M., Andersen, M. S. and Cuthbert, M. O.:
584 Understanding connected surface-water/groundwater systems using Fourier analysis of
585 daily and sub-daily head fluctuations, *Hydrogeol. J.*, 23(1), 143–159, doi:10.1007/s10040-
586 014-1182-5, 2015.
- 587 Adamson, L. and Loudon, A.: *Wagga Geological Sheet, SI/55-15*, 1st edition, 1:250000, 1966.
- 588 Auger, F. and Flandrin, P.: Improving the readability of time-frequency and time-scale
589 representations by the reassignment method, *IEEE Trans. Signal Process.*, 43(5), 1068–1089,
590 doi:10.1109/78.382394, 1995.
- 591 Baker, A., Bradley, C., Phipps, S. J., Fischer, M., Fairchild, I. J., Fuller, L., Spötl, C. and Azcurra,
592 C.: Millennial-length forward models and pseudoproxies of stalagmite $\delta^{18}\text{O}$: an example
593 from NW Scotland, *Clim. Past*, 8(4), 1153–1167, doi:10.5194/cp-8-1153-2012, 2012.
- 594 Baker, A. and Brunsdon, C.: Non-linearities in drip water hydrology: an example from Stump
595 Cross Caverns, Yorkshire, *J. Hydrol.*, 277(3-4), 151–163, doi:10.1016/S0022-1694(03)00063-
596 5, 2003.
- 597 Baldini, J. U. L., McDermott, F., Baker, A., Baldini, L. M., Matthey, D. P. and Railsback, L. B.:
598 Biomass effects on stalagmite growth and isotope ratios: A 20th century analogue from
599 Wiltshire, England, *Earth Planet. Sci. Lett.*, 240(2), 486–494, doi:10.1016/j.epsl.2005.09.022,
600 2005.
- 601 Baldini, J. U. L., McDermott, F., Baldini, L. M., Ottley, C. J., Linge, K. L., Clipson, N. and Jarvis,
602 K. E.: Identifying short-term and seasonal trends in cave drip water trace element
603 concentrations based on a daily-scale automatically collected drip water dataset, *Chem.*
604 *Geol.*, 330-331, 1–16, doi:10.1016/j.chemgeo.2012.08.009, 2012.



- 605 Bradley, C., Baker, A., Jex, C. N. and Leng, M. J.: Hydrological uncertainties in the modelling
606 of cave drip-water $\delta^{18}O$ and the implications for stalagmite palaeoclimate reconstructions,
607 *Quat. Sci. Rev.*, 29(17-18), 2201–2214, doi:10.1016/j.quascirev.2010.05.017, 2010.
- 608 Burgess, S. S. O., Adams, M. A., Turner, N. C., White, D. A. and Ong, C. K.: Tree roots:
609 Conduits for deep recharge of soil water, *Oecologia*, 126(2), 158–165,
610 doi:10.1007/s004420000501, 2001.
- 611 Carbon, B. A., Bartle, G. A., Murray, A. M. and Macpherson, D. K.: The Distribution of Root
612 Length, and the Limits to Flow of Soil Water to Roots in a Dry Sclerophyll Forest, *For. Sci.*,
613 26(4), 656–664, 1980.
- 614 Coleborn K., Spate A., Tozer, M., Andersen M. S., Fairchild I. J., MacKenzie, B., Treble P. C.,
615 Meehan, S., Baker, A., Baker A., Effects of wildfire on long-term soil CO₂ concentration:
616 implications for karst processes, *Envi. Earth. Sci*, doi:10.1007/s12665-015-4874-9.
- 617 Collister, C. and Matthey, D.: Controls on water drop volume at speleothem drip sites: An
618 experimental study, *J. Hydrol.*, 358, 259–267, doi:10.1016/j.jhydrol.2008.06.008, 2008.
- 619 Crombie, D. S.: Root Depth, Leaf Area and Daytime Water Relations of Jarrah (*Eucalyptus*
620 *marginata*) Forest Overstorey and Understorey during Summer Drought, *Aust. J. Bot.*,
621 40(1988), 113–22, doi:10.1071/BT9920113, 1992.
- 622 Cuthbert, M., Baker, A., Jex, C., Graham, P., Treble, P., Andersen, M. and Acworth, I.: Drip
623 water isotopes in semi-arid karst: Implications for speleothem paleoclimatology, *Earth*
624 *Planet. Sci. Lett.*, 395, 194–204, doi:10.1016/j.epsl.2014.03.034, 2014a.
- 625 Cuthbert, M. O., Rau, G. C., Andersen, M. S., Roshan, H., Rutledge, H., Marjo, C. E.,
626 Markowska, M., Jex, C. N., Graham, P. W., Mariethoz, G., Acworth, R. I. and Baker, a:
627 Evaporative cooling of speleothem drip water., *Sci. Rep.*, 4, 5162, doi:10.1038/srep05162,
628 2014b.
- 629 Daubechies, I., Lu, J. and Wu, H. T.: Synchrosqueezed wavelet transforms: An empirical
630 mode decomposition-like tool, *Appl. Comput. Harmon. Anal.*, 30(2), 243–261,
631 doi:10.1016/j.acha.2010.08.002, 2011.
- 632 Dawson, T. E. and Pate, J. S.: Seasonal water uptake and movement in root systems of
633 Australian phraeatophytic plants of dimorphic root morphology: a stable isotope
634 investigation, *Oecologia*, 107(1), 13–20, doi:10.1007/BF00582230, 1996.
- 635 Fairchild, I. J. and Baker, A.: *Speleothem Science: From Process to Past Environments*, 1st
636 ed., Wiley-Blackwell., 2012.
- 637 Fairchild, I. J., Borsato, A., Tooth, A. F., Frisia, S., Hawkesworth, C. J., Huang, Y. and
638 Mcdermott, F.: Controls on trace element $\delta Sr - Mg$ / compositions of carbonate cave
639 waters : implications for speleothem climatic records, 2000.
- 640 Farrington, P., Turner, J. and Gailitis, V.: *Eucalyptus marginata*, *Trees*, 11, 9–15, 1996.
- 641 Genty, D. and Deflandre, G.: Drip flow variations under a stalactite of the Pere Noel cave
642 (Belgium). Evidence of seasonal variations and air pressure constraints, *J. Hydrol.*, 211(1-4),



- 643 208–232, doi:10.1016/S0022-1694(98)00235-2, 1998.
- 644 Gribovszki, Z., Szilágyi, J. and Kalicz, P.: Diurnal fluctuations in shallow groundwater levels
645 and streamflow rates and their interpretation - A review, *J. Hydrol.*, 385(1-4), 371–383,
646 doi:10.1016/j.jhydrol.2010.02.001, 2010.
- 647 Hu, C., Henderson, G. M., Huang, J., Chen, Z. and Johnson, K. R.: Report of a three-year
648 monitoring programme at Heshang Cave, Central China, *Int. J. Speleol.*, 37(October), 143–
649 151, doi:10.5038/1827-806X.37.3.1, 2008.
- 650 Jex, C. N., Mariethoz, G., Baker, A., Graham, P., Andersen, M. S., Acworth, I., Edwards, N.
651 and Azcurra, C.: Spatially dense drip hydrological monitoring and infiltration behaviour at
652 the Wellington Caves, South East Australia, *Int. J. Speleol.*, 41(2), 283–296, 2012.
- 653 Mahmud, K., Mariethoz, G., Baker, A., Treble, P. C., Markowska, M. and McGuire, E.:
654 Estimation of deep infiltration in unsaturated limestone environments using cave LiDAR and
655 drip count data, *Hydrol. Earth Syst. Sci. Discuss.*, 12(9), 8891–8925, doi:10.5194/hessd-12-
656 8891-2015, 2015.
- 657 Mariethoz, G., Baker, A., Sivakumar, B., Hartland, A. and Graham, P.: Chaos and irregularity
658 in karst percolation, *Geophys. Res. Lett.*, 39(23), n/a–n/a, doi:10.1029/2012GL054270, 2012.
- 659 Markowska, M., Baker, A., Treble, P. C., Andersen, M. S., Hankin, S., Jex, C. N., Tados, C. V.
660 and Roach, R.: Unsaturated zone hydrology and cave drip discharge water response:
661 Implications for speleothem paleoclimate record variability, *J. Hydrol.*,
662 doi:10.1016/j.jhydrol.2014.12.044, 2015.
- 663 Markowska, M., Baker, A., Andersen, M. S., Jex, C. N., Cuthbert, M. O., Rau, G. C., Graham, P.
664 W., Rutledge, H., Mariethoz, G., Marjo, C. E., Treble, P. C., Edwards, N., Semi-arid zone caves:
665 Evaporation and hydrological controls on $\delta^{18}\text{O}$ drip water composition and implications for
666 speleothem paleoclimate reconstruction, *Quat. Sci. Rev.*, 131,
667 doi:10.1016/j.quascirev.2015.10.024, 2016.
- 668 McDonald, J.: The 2002–2003 El Niño recorded in Australian cave drip waters: Implications
669 for reconstructing rainfall histories using stalagmites, *Geophys. Res. Lett.*, 31(22),
670 doi:10.1029/2004GL020859, 2004.
- 671 McDonald, J. and Drysdale, R.: Hydrology of cave drip waters at varying bedrock depths
672 from a karst system in southeastern Australia, *Hydrol. Process.*, 1748(March), 1737–1748,
673 doi:10.1002/hyp, 2007.
- 674 Merritt, M. L.: Estimating Hydraulic Properties of the Floridan Aquifer System by Analysis of
675 Effects, Collier and Hendry Counties, Florida, Secretary, 70, 2004.
- 676 Meyer, K. W., Feng, W., Breecker, D. O., Banner, J. L. and Guilfoyle, A.: Interpretation of
677 speleothem calcite $\delta^{13}\text{C}$ variations: Evidence from monitoring soil CO_2 , drip water, and
678 modern speleothem calcite in central Texas, *Geochim. Cosmochim. Acta*, 142, 281–298,
679 doi:10.1016/j.gca.2014.07.027, 2014.
- 680 Noronha, A. L., Johnson, K. R., Southon, J. R., Hu, C., Ruan, J. and McCabe-Glynn, S.:
681 Radiocarbon evidence for decomposition of aged organic matter in the vadose zone as the



- 682 main source of speleothem carbon, *Quat. Sci. Rev.*, 127, 37–47,
683 doi:10.1016/j.quascirev.2015.05.021, 2015.
- 684 O’Grady, A P., Eamus, D. and Hutley, L. B.: Transpiration increases during the dry season:
685 patterns of tree water use in eucalypt open-forests of northern Australia, *Tree Physiol.*,
686 19(9), 591–597, doi:10.1093/treephys/19.9.591, 1999.
- 687 Peel, M. C., Finlayson, B. L. and McMahon, T. A: Updated world map of the K oppen-Geiger
688 climate classification, *Hydrol. Earth Syst. Sci. Discuss.*, 4, pp. 439–473, doi:10.5194/hess-11-
689 1633-2007, 2007.
- 690 Proctor, C. J., Baker, A., Barnes, W. L. and Gilmour, M. A.: A thousand year speleothem
691 proxy record of North Atlantic climate from Scotland, *Clim. Dyn.*, 16(10-11), 815–820,
692 doi:10.1007/s003820000077, 2000.
- 693 Rau, G. C., Cuthbert, M. O., Andersen, M. S., Baker, A., Rutledge, H., Markowska, M., Roshan,
694 H., Marjo, C. E., Graham, P. W. and Acworth, R. I.: Controls on cave drip water temperature
695 and implications for speleothem-based paleoclimate reconstructions, *Quat. Sci. Rev.*, 127,
696 1–18, doi:10.1016/j.quascirev.2015.03.026, 2015.
- 697 Rutledge, H., Baker, A., Marjo, C. E., Andersen, M. S., Graham, P. W., Cuthbert, M. O., Rau, G.
698 C., Roshan, H., Markowska, M., Mariethoz, G. and Jex, C. N.: Dripwater organic matter and
699 trace element geochemistry in a semi-arid karst environment: Implications for speleothem
700 paleoclimatology, *Geochim. Cosmochim. Acta*, 135, 217–230,
701 doi:10.1016/j.gca.2014.03.036, 2014.
- 702 Scott, T. M., Campbell, K. M., Rupert, F. R., Arthur, J. D., Missimer, T. M., Lloyd, J. M., Yon, J.
703 W., and Duncan, J. G., 2001, *Geologic Map of the State of Florida*, Florida Geological Survey
704 & Florida Department of Environmental Protection, Map Series 146.
- 705 Sondag, F., Van Ruymbeke, M., Soubiès, F., Santos, R., Somerhausen, A., Seidel, A. and
706 Boggiani, P.: Monitoring present day climatic conditions in tropical caves using an
707 Environmental Data Acquisition System (EDAS), *J. Hydrol.*, 273(1-4), 103–118,
708 doi:10.1016/S0022-1694(02)00362-1, 2003.
- 709 Spate, A.: *Karst Values*, Hurstville., 2002.
- 710 Stern, H., Hoedt, G. de and Ernst, J.: Objective classification of Australian Climates, *Bur.*
711 *Meteorol.* [online] Available from:
712 http://www.bom.gov.au/climate/enviro/other/koppen_explain.shtml (Accessed 15
713 October 2013), 2012.
- 714 Thakur, G., Brevdo, E., Fučkar, N. S. and Wu, H. T.: The Synchrosqueezing algorithm for time-
715 varying spectral analysis: Robustness properties and new paleoclimate applications, *Signal*
716 *Processing*, 93(5), 1079–1094, doi:10.1016/j.sigpro.2012.11.029, 2013.
- 717 Tooth, A. F. and Fairchild, I. J.: Soil and karst aquifer hydrological controls on the
718 geochemical evolution of speleothem-forming drip waters, Crag Cave, southwest Ireland, *J.*
719 *Hydrol.*, 273(1-4), 51–68, doi:10.1016/S0022-1694(02)00349-9, 2003.
- 720 Treble, P., Markowska, M., Tadros, C., Jex, C., Coleborn, K., Dredge, J., Baker, A., Roach, R.



- 721 and Spate, A.: Reconstructing past environmental change at Yarrangobilly Caves, pp. 83–88.,
722 2013a.
- 723 Treble, P. C., Bradley, C., Wood, A., Baker, A., Jex, C. N., Fairchild, I. J., Gagan, M. K., Cowley,
724 J. and Azcurra, C.: An isotopic and modelling study of flow paths and storage in Quaternary
725 calcarenite, SW Australia: implications for speleothem paleoclimate records, *Quat. Sci. Rev.*,
726 64, 90–103, doi:10.1016/j.quascirev.2012.12.015, 2013b.
- 727 Treble, P. C., Fairchild, I. J., Griffiths, A., Baker, A., Meredith, K. T., Wood, A. and McGuire, E.:
728 Impacts of cave air ventilation and in-cave prior calcite precipitation on Golgotha Cave
729 dripwater chemistry, southwest Australia, *Quat. Sci. Rev.*, 127,
730 doi:10.1016/j.quascirev.2015.06.001, 2015.
- 731 Treble, P. C., Fairchild, I. J., Baker, A., Meredith, K. M., Andersen, M. S., Salmon, S. U.,
732 Bradley, C., Wynn, P. M., Hankin, S., Wood, A. and McGuire, E.: Roles of bioproductivity,
733 transpiration and fire in an eight-year record of cave dripwater chemistry from a forested
734 catchment, southwest Australia, n.d.
- 735 Tremaine, D. M. and Froelich, P. N.: Speleothem trace element signatures: A hydrologic
736 geochemical study of modern cave dripwaters and farmed calcite, *Geochim. Cosmochim.*
737 *Acta*, 121, 522–545, doi:10.1016/j.gca.2013.07.026, 2013.
- 738 Wong, C. and Banner, J. L.: Response of cave air CO₂ and drip water to brush clearing in
739 central Texas: Implications for recharge and soil CO₂ dynamics, *J. Geophys. Res.*, 115,
740 doi:10.1029/2010JG001301, 2010.
- 741 Worboys, G.: Kosciusko National Park Geology and Geomorphology, National Parks and
742 Wildlife Services, Sydney., 1982.
- 743